Running title: Advanced lesion symptom mapping analyses

Advanced lesion symptom mapping analyses and implementation as BCBtoolkit

Foulon C[a,b,c*], Cerliani L[a,b,c], Kinkingnéhun S[a], Levy R[b], Rosso C[c,d], Urbanski M[a,b,c], Volle E[a,b,c], Thiebaut de Schotten M[a,b,c*]

[a] Brain Connectivity and Behaviour Group, Brain and Spine Institute, Paris France.

[b] Frontlab, Institut du Cerveau et de la Moelle épinière (ICM), UPMC UMRS 1127, Inserm U 1127, CNRS UMR 7225, Paris, France.

[c] Centre de Neuroimagerie de Recherche CENIR, Groupe Hospitalier Pitié-Salpêtrière, Paris, France.

[d] APHP, Urgences Cérébro-Vasculaires, Groupe Hospitalier Pitié-Salpêtrière, Paris, France.

* Corresponding authors hd.chrisfoulon@gmail.com and michel.thiebaut@gmail.com

Running title: Advanced lesion symptom mapping analyses

Abstract: Patients with brain lesions provide a unique opportunity to understand the functioning of the human mind. However, brain lesions, even when focal, have local and remote effects impacting functionally and structurally connected circuits. Here we deliver for the first time a set of complementary solutions to measure the consequences of a given lesion upon the affected circuits. Our methods were applied to 37 patients with a focal brain lesion, revealing a large set of disconnected brain regions, which significantly impacted category fluency performance. These regions corresponded to areas that are classically considered as functionally engaged in verbal fluency and categorization tasks. These areas were organized into large functional networks, including the left ventral fronto-parietal network, whose cortical thickness proportionally decreased with performance on category fluency. Hence, the methods presented here reveal the remote effects of brain lesions, provide for the identification of the affected networks, and strengthen understanding of their relationship with cognitive and behavioural measures.

Recent advances in neuroimaging techniques, allowed for the further examination of the structural and the functional organization of the human brain. While diffusion weighted imaging (DWI) tractography (Jones *et al.*, 1999) depicts how brain areas are connected together, functional magnetic resonance imaging (*f*MRI) measures the activity within and interaction between brain areas in the elaboration of function (Logothetis, 2008). While these methods have been successfully applied to the healthy human brain, they remain underused in patients with a brain lesion.

Patients with brain lesions provide a unique opportunity to understand the functioning of the human mind. Lesion symptom mapping analyses traditionally assume that visible and directly damaged areas are responsible for a patient's symptoms (Broca, 1861; Damasio and Damasio, 1989; Rorden *et al.*, 2007; Mah *et al.*, 2014). Following this logic, the areas that are the most frequently damaged by the lesion are considered as the neurological substrate for the function. Previous studies employing this method have pinpointed critical areas dedicated to, for example, language production (Bates *et al.*, 2003), comprehension (Dronkers *et al.*, 2004), spatial awareness (Husain and Kennard, 1996; Karnath *et al.*, 2001; Mort *et al.*, 2003; Bird *et al.*, 2006) or other high-level cognitive functions (Coulthard *et al.*, 2008; Volle *et al.*, 2008; Badre *et al.*, 2009; Volle *et al.*, 2013). However, anatomical disconnections between regions are also important considerations for the exploration of cognitive deficit (Geschwind, 1965a, b). Dysfunction of distant areas that are connected to the lesion have also been reported in *f*MRI studies. They have shown that the networks are disrupted even by distant lesions through disconnection and diaschisis mechanisms (Finger *et al.*, 2004; Corbetta *et al.*, 2005; Carrera and Tononi, 2014).

Disconnections and diaschisis can have an impact upon distant regions in several respects. When disconnected from its inputs and outputs, a region can no longer contribute to the elaboration of the supported function. Additionally, once deprived from its inputs and outputs, a neuron will reduce its size or die through a mechanism called apoptosis, a programmed cell death, which occurs when a neuron becomes unable to receive or send information (Bredesen, 1995; Capurso *et al.*, 1997). Hence, a white matter disconnection leads to both functional and anatomical changes that extend well beyond the visible damage. New approaches are therefore required to capture the long-range effects that follow brain

disconnections.

In response to this need, we provide here a set of complementary solutions to measure both the circuit, and the subsequent change within the circuit that is affected by a lesion in a given location. We applied these methods to 37 patients with a focal brain lesion. We first assessed the risk of disconnection in well-known white matter tracts and tested their relationship with category fluency performance. We then developed a tractography-based approach in order to produce maps of the areas that are directly disconnected by the lesion and tested their relationship with category fluency performance. We additionally calculated the functional connectivity of these areas to reveal the whole network of directly and indirectly connected regions that participate in category fluency. We finally explored potential microstructural changes in the latter disconnected regions, including for neuronal loss or synaptic and dendritic degeneration derived from MR-based measures of cortical thickness and resting state *f*MRI entropy.

Methods

Participants and Category fluency task

Thirty-seven right-handed patients (French-native speakers; 19 females; mean age 48 years, age ranging from 23 to 75 years) who presented with a frontal lesion at the chronic stage (> 3 months) were included in this study. The patients were recruited from the stroke unit and the neuroradiology department at Salpêtrière Hospital, the neurological unit at Saint-Antoine Hospital and the neuroradiology department at Lariboisière Hospital in Paris. Patients with a history of psychiatric or neurological disease, drug abuse, or MRI contraindications were not included. Additionally, we gathered data from 54 healthy participants (French-native speakers; 27 females; mean age 45.8 years, age ranging from 22 to 71 years) in order to constitute a normative group.

All participant performed a category fluency task (Lezak, 1995) in french. They were instructed to say as many animals' names as quickly as possible during a period of 60 seconds. Results were recorded by a trained neuropsychologist (M.U.). Repetition and declination of the same animal were not taken into account in the final category fluency score.

Magnetic resonance imaging

An axial three-dimensional magnetization prepared RApid gradient echo (MPRAGE) dataset covering the whole head was acquired for each participant (176 slices, voxel resolution = 1 × 1 × 1 mm, echo time = 3 msec, repetition time = 2300 msec, flip angle = 9°). Additionally, the same participants underwent a *f*MRI session of resting state. During the resting state session, participants were instructed to relax, keep their eyes closed but to avoid falling asleep.

Functional images were obtained using T2-weighted echo-planar imaging (EPI) with blood oxygenation level-dependent contrast using SENSE imaging an echo time of 26 msec and a repetition time of 3000 msec, each dataset comprised 32 axial slices acquired continuously in ascending order covering the entire cerebrum with a voxel resolution of 2 x 2 x 3 mm.

Finally, diffusion weighted imaging was also acquired for 10 participants of the normative group (French-native male speakers; mean age 56.44 years, age ranging from 45 to 66 years) and consisted in a total of 70 near-axial slices acquired using a fully optimised acquisition sequence for the tractography of diffusion-weighted imaging (DWI), which provided isotropic (2 × 2 × 2 mm) resolution and coverage of the whole head with a posterior-anterior phase of acquisition. The acquisition was peripherally-gated to the cardiac cycle (Jones *et al.*, 2002) with an echo time = 85 msec. We used a repetition time equivalent to 24 RR. At each slice location, 6 images were acquired with no diffusion gradient applied. Additionally, 60 diffusion-weighted images were acquired, in which gradient directions were uniformly distributed on the hemisphere with electrostatic repulsion. The diffusion weighting was equal to a b-value of 1500 sec mm^{-2}.

Stereotaxic space registration

As spatial normalisation can be affected by the presence of a brain lesion, additional processing are required before calculating the normalisation. To this purpose, the first step was to produce an enantiomorphic filling of the damaged area (Nachev *et al.*, 2008). Each patient lesions (or signal abnormalities due to the lesion) were manually segmented (using FSLview; http://fsl.fmrib.ox.ac.uk) and replaced symmetrically by the healthy tissue of the contralateral hemisphere. Enantiomorphic T1 images were fed into FAST (Zhang *et al.*, 2001) for estimation of the bias field and subsequent correction of RF inhomogeneities. This

improves the quality of the automated skull stripping performed using bet (Smith, 2002) and the registration to the MNI152 using affine and diffeomorphic deformations (Avants *et al.*, 2011). The original T1 images (non enantiomorphic) were registered to the MNI152 space using the same affine and diffeomorphic deformations as calculated above. Consecutively, lesions were segmented again in the MNI152 space under the supervision of an expert neurologist (E.V.). This method has been made freely available as the tool 'Normalisation' as part of BCBtoolkit (http://toolkit.bcblab.com).

White matter tracts disconnection

Each patient's lesion was compared with an atlas of white matter tracts (Rojkova *et al.*, 2016), indicating for each voxel, the probability of finding a white matter tract such as the arcuate fasciculus, the frontal aslant tract or the superior longitudinal fasciculus in the MNI152. We considered a tract to be disconnected when this risk was estimated to be above 50% (Thiebaut de Schotten *et al.*, 2014). This method is freely available as part of the BCBtoolkit (http://toolkit.bcblab.com) and referred to as 'Tractotron'.

Direct disconnection of brain areas: structural connectivity network

This approach employed a set of 10 healthy controls diffusion weighted imaging datasets to track fibers passing through each lesion. For each participant, tractography was estimated as indicated in (Thiebaut de Schotten *et al.*, 2011).

Patients' lesions in the MNI152 space were registered to each control native space using affine and diffeomorphic deformations (Avants *et al.*, 2011), and subsequently, used as seed for the tractography in Trackvis (http://trackvis.org). Tractography from the lesions were transformed in visitation maps (Thiebaut de Schotten *et al.*, 2011), binarised and brought to the MNI152 using the inverse of precedent deformations. Finally, we produced a percentage overlap map by summing at each point in MNI space the normalized visitation map of each healthy subject. Hence, in the resulting disconnectome map, the value in each voxel took into account the inter-individual variability of tract reconstructions in controls, and indicated a probability of disconnection from 0 to 100% for a given lesion. This procedure was repeated for all lesions, allowing the construction of a disconnectome map for each patient/lesion. These steps were automatised in the tool 'disconnectome map' as parts of the BCBtoolkit.

Thereafter, we used AnaCOM2 as parts of the BCBtoolkit in order to perform non-parametric Mann Whitney statistics (R Core Team 2016, https://www.r-project.org) on the disconnectome maps. AnaCOM2 is a cluster-based lesion approach facilitating the identification of the location of brain lesions that are associated with a given deficit, i.e. the regions that are critical for a given function. Compared to standard VLSM (Bates *et al.*, 2003), AnaCOM2 regroups voxels with the same distribution of neuropsychological scores into clusters of voxels. Additionally, AnaCOM2 performs comparisons between patients and controls as a first step in order to avoid drastic reduction of statistical power when two or more non-overlapping areas are responsible for patients reduced performance (Kinkingnehun *et al.*, 2007). AnaCOM2 resulted in a statistical map that reveals, for each cluster, the significance of a deficit in patients undertaking a given task as compared to controls. Between patients' comparisons were also performed in significant areas as post-hoc comparisons. Reported p-values were Bonferroni-Holms corrected for multiple comparisons.

Indirect disconnection of brain areas: functional connectivity network

Rs-*f*MRI images were first motion corrected using MCFLIRT (Jenkinson *et al.*, 2002), then corrected for slice timing, smoothed with a full half width maximum equal to 1.5 times the largest voxel dimension and finally filtered for low temporal frequencies using a gaussian-weighted local fit to a straight line. These steps are available in Feat as part of FSL package (Woolrich *et al.*, 2009).

Rs-*f*MRI images were linearly registered to the enantiomorphic T1 images, and subsequently to the MNI152 template (2mm) using affine transformation. Confounding signals were discarded from rs-*f*MRI by regressing out a confound matrix from the functional data. The confound matrix included the estimated motion parameters obtained from the previously performed motion correction, the first eigenvariate of the white matter and cerebrospinal fluid as well as their first derivative. Eigenvariates can easily be extracted using fslmeants combined with the --eig option. White matter and cerebrospinal fluid eigenvariates were extracted using masks based on the T1 derived 3-classes segmentation thresholded to a probability value of 0.9, registered to the rs-*f*MRI images and binarized. Finally, the first derivative of the motion parameters, white matter and cerebrospinal fluid signal was calculated by linear convolution between their time course and a [-1 0 1] vector.

For each control participant, we extracted the time course that corresponded to each

significant cluster and which was identified by the statistical analyses of the disconnectome maps. These time courses were subsequently correlated to the rest of the brain so as to extract seed-based resting-state networks. In order to obtain the most representative networks at the group level, for each seed-based resting-state network, we calculated the median network across the group. All these steps were automatised and made available as the 'Funcon' tool as part of the BCBtoolkit.

Visual inspection revealed that several of these resting state networks shared a very similar distribution of activations. Therefore, an 'activation' matrix was derived from the seed-based resting-state networks. This matrix consisted of columns that indicated each seed-based resting-state network, and rows that represented the level of activation for each voxel in the cortex. This 'activation' matrix was entered into a principal component analysis in SPSS (SPSS, Chicago, IL) using a covariance matrix and varimax rotation (with a maximum of 50 iterations for convergence), in order to estimate the number of principal components to extract for each function. Components were plotted according to their eigenvalue (y) (Lower left panel in **Fig. 4**) and we applied a scree test to separate the principal from residual components. This analysis revealed that three factors were enough to explain more than 82% of the variance of the calculated seed-based resting-state networks. Finally, brain regions having a statistically significant relationship with the three components were detected using a linear regression with 5.000 permutations, in which the eigenvalues of the three components represented the independent variable and the seed-based resting-state networks the dependent variable. Results were Family Wise Error (FWE) corrected for multiple comparisons, and projected onto the average 3D rendering of the MNI152 template in the top panel of **Fig. 4**.

Microstructural changes in disconnected regions

A distant lesion can affect cortical microstructure remotely. Conscious of this, we attempted to estimate these structural changes and their relationship with category fluency within each functional network. To this aim, we explored the properties of each functional network using two complementary measures: T1w-based cortical thickness to identify fine local volumetric changes and the Shannon entropy of rs-*f*MRI as a surrogate for the local complexity of the neural networks (Sokunbi *et al.*, 2013). Each functional network was thresholded and binarized at r>0.3 and used as masks to extract cortical thickness and entropy.

For the cortical thickness, a registration-based method (Diffeomorphic Registration based

Cortical Thickness, DiReCT) was employed (Das *et al.*, 2009) from the T1-weighted imaging dataset. The first step of this method consisted in creating two two-voxel thick sheets, one lying just between the grey matter and the white matter and the second laying between the grey matter and the cerebrospinal fluid. Then, the grey/white interface was expanded to the grey/cerebrospinal fluid interface using diffeomorphic deformation estimated with ANTs. The registration produced a correspondence field that allows an estimate of the distance between the grey/white and the grey/cerebrospinal fluid interfaces, and thus corresponded to an estimation of cortical thickness. This approach has good scan-rescan repeatability and good neurobiological validity as it can predict with a high statistical power the age and gender of the participants (Tustison *et al.*, 2014).

Shannon entropy was extracted from the previously preprocessed rs-*f*MRI using the following formula: ·(-i * log(i))/n whereby I indicate the intensity in the voxels and n the number of voxels measured.

FSLstats was employed to extract the average cortical thickness and resting state *f*MRI entropy for each network. Statistical analysis was performed using SPSS software (SPSS, Chicago, IL). In our analysis, Gaussian distribution of the data was not confirmed for the cortical thickness and the entropy measures using the Shapiro–Wilk test. Therefore, Bivariate Spearman rank correlation coefficient analyses were performed between the cortical thickness or entropy measurement of each functional network and each patient's category fluency performance. Correlation significant at $P < 0.0041$ survives Bonferroni correction for multiple comparisons (12 networks).

Results

White matter tracts disconnection

Patients' lesions were compared to an atlas of white matter connections in order to identify the probability of tract disconnections. A Kruskall Wallis test indicated that for each tract, both preserved and disconnected, patients and control participants showed a significantly different performance on the category fluency test (all $p < 0.001$, full statistics reported in **Table 1**). Between patients, post-hoc comparisons revealed that a disconnection of the left anterior ($U = 28.5$; $p = 0.0464$) and long segment ($U = 31.5$; $p = 0.0464$) of the arcuate fasciculus was decisively associated with a poorer performance in category fluency (**Fig. 1**).

These results indicate that poor performance measured in patients with brain damage can significantly be associated with white matter tract disconnections.

Direct disconnection of brain areas

Using tractography in a group of 10 healthy controls, the registered lesions were used as a seed to reveal white matter tracts that passed through the injured area so as to produce maps of disconnection, later referred to as disconnectome maps. Category fluency scores were attributed to each patient's disconnectome map (see **Fig. 2a**). Results were further statistically assessed in order to identify areas that, when deafferented due to a disconnection mechanism, lead to a significant decrease in performance in category fluency when compared to controls.

The following results are Bonferroni-Holmes corrected for multiple comparisons. Main cortical areas in the left hemisphere included the pre-supplementary motor area (Cluster size = 1449; Mann Whitney U = 88.5 ; p = 0.025), the anterior portion of the intraparietal sulcus (Cluster size = 1143; U = 18 ; p = 0.030), anterior (Cluster size = 837; U = 304 ; p = 0.025) and the middle (Cluster size = 898; U = 95.5 ; p = 0.014) cingulate gyrus, the middle frontal gyrus (Cluster size = 829; U = 81.5 ; p = 0.005), the pars opercularis (Cluster size = 5314; U = 16 ; p = 0.025).

In the right hemisphere the pre-supplementary motor area (Cluster size = 1050; U = 50.5 ; p = 0.014), the middle frontal gyrus (Cluster size = 552; U = 54 ; p = 0.018), the anterior (Cluster size = 572; U = 44.5 ; p = 0.009) and the middle (Cluster size = 817; U = 317 ; p = 0.041) cingulate gyrus were also involved (**Fig. 2b**)

Subcortical areas in the left hemisphere involved the caudate, the putamen and several ventral thalamic nuclei including the ventral anterior (VA), the ventrolateral anterior (VLa) and the ventrolateral posterior (VLp) as a part of the same cluster (Cluster size = 5314; U = 16 ; p = 0.025)

In right hemisphere the caudate (Cluster size = 527; U = 310 ; p = 0.031) , the putamen

(Cluster size = 1212; U = 225 ; p = 0.033) and the ventral thalamic nuclei (Cluster size = 935; U = 202 ; p = 0.025) were similarly involved (**Fig. 2b**).

Additionally, between patients (i.e. connected and disconnected, Bonferroni-Holmes corrected for multiple comparisons) comparisons confirmed the critical involvement of the preSMA (U = 88, p = 0.0456) the middle frontal gyrus (U = 75, p = 0.0208), the pars opercularis (U = 31, p = 0.0132) and the intra-parietal sulcus (U = 38, p = 0.0245) in the left hemisphere. The preSMA (U = 62; p = 0.039) was also involved in the right hemisphere (**Fig. 2c)**.

fMRI Meta-analyses

We further examined whether the disconnected areas in patients with poor performance are functionally engaged in tasks related to fluency and categorization using a meta-analysis approach (http://neurosynth.org) (Yarkoni *et al.*, 2011).

The result indicates that disconnected areas reported as significantly contributing to category fluency performance in patients are classically activated by functional MRI tasks requiring either fluency or categorization in healthy controls (**Fig. 3**).

Microstructural changes in disconnected regions

Additional exploratory analyses investigated structural changes related to the disconnections. We estimated these changes using two complementary measures: T1w based cortical thickness to identify fine local volumetric changes and the Shannon entropy of rs-*f*MRI as a surrogate for the local complexity of the neural networks (Sokunbi *et al.*, 2013).

When compared to controls, disconnected patients showed a reduced cortical thickness in the left pars opercularis (U = 44; p = 0.005), the middle frontal gyrus (U = 172; p = 0.019), the pre-supplementary motor area (U = 168; p = 0.034), the intraparietal sulcus (U = 59; p = 0.015) and the right middle cingulate gyrus (U = 223 ; p = 0.001). When compared to patients with no disconnection, solely the right middle cingulate gyrus survived the Bonferroni Holmes correction for multiple comparison (U = 67; p = 0.004). When compared to controls, disconnected patients showed reduced entropy for all regions (all $p < 0.05$, except for right

middle frontal gyrus). However, when compared to patients with no disconnection, none of the comparisons survived the Bonferroni-Holmes correction for multiple comparisons. Uncorrected p values are reported as an indication in **table 2, and bar chart in supplementary Fig. 1.**

None of these measures correlated significantly with the fluency performance.

Indirect disconnection of brain areas

As the disconnectome mapping method cannot measure the indirect disconnection produced by a lesion (i.e. it fails to measure the disconnection in a region that is not directly, anatomically connected to a damaged area, but that nonetheless remains a part of the same large network of functionally connected areas), we therefore employed functional connectivity in healthy controls. This allowed us to reveal the entire network of regions that are functionally connected to the areas that were reported as contributing significantly to the category fluency performance when directly disconnected. When compared to tractography, functional connectivity, has the added advantage of revealing the areas that contribute to the network through both direct, as well as indirect, structural connections.

Principal component analysis indicated that the significant areas contributing to category fluency performance belonged to 3 main functional networks (**Fig. 4**), which accounted for more than 80% of the total variance of the functional connectivity results.

The left cingulate clusters (anterior and middle), the right anterior cingulate, the middle frontal gyrus, the thalamus, and the operculum all belonged to the cingulo-opercular network (CO,Sadaghiani and D'Esposito, 2015) including also the right preSMA, posterior cingulate and the rostral portion of the middle frontal gyrus.

The middle of the cingulate gyrus and the striatum in the right hemisphere both belonged to a cortico-striatal network (CS,Voorn *et al.*, 2004) involving the right thalamus and striatum.

Finally, the left MFg, preSMA, IPs, the pars opercularis, the thalamus and the striatum were all involved in a larger, left ventral fronto-parietal network, which also included other areas such as the right preSMA, the frontal eye field and the temporo-parietal junction (VFP,Smith *et al.*, 2009).

Additional analyses investigated the differences in the functional connectivity of these networks relative to the disconnected status of areas involved in category fluency. Between patients (i.e. connected and disconnected) comparisons revealed significantly lower functional connectivity in the left VFP network (U = 54, p = 0.006) and in the CS network (U = 63, p = 0.027) when anatomically disconnected. The CO network, however, did not show any significant difference (U = 40, p = 0.213). Moreover, the strength of the functional connectivity for each patient did not correlate significantly with the fluency performance.

In order to further assess the integrity of the whole network of regions that were functionally connected to the areas reported as having significantly contributed to the category fluency performance, we also extracted the cortical thickness and entropy from the regions that were functionally connected to the disconnected areas. Correlation analyses indicated that a thinner cortex in the ventral fronto-parietal network seeded from the left MFg (Spearman Rho = .464 ± 0.341; p = .004) , IPs (Rho = .475 ± 0.341 ; p = .003) and left oper./striatum/thalamus (Rho = .512 ± 0.341 ; p = .001) corresponded to a proportionally reduced performance in category fluency (**Fig. 5**). Additionally, a thinner cortical thickness in the left preSMA functional network (Rho = .376 ± 0.341 ; p = .024) and a higher rs-*f*MRI entropy (Rho = – .420 ± 0.370 ; p = .019) in the mid cingulate gyrus functional network was associated with poorer performance in category fluency. These two last results, however, did not survive Bonferroni-Holmes correction for multiple comparisons.

Discussion

A large set of complementary methods can capture the impact of lesions on distant regions and expose the subsequent consequences upon a patients' neuropsychological performance. Several of these methods are built directly into the BCBtoolkit, which can be applied to measure some of the pathophysiological mechanisms that cause cognitive deficits, and assess the relationship between these mechanisms and their consequential effect. Here we evaluated the risk of disconnection of classically defined white matter tracts and tested their relationship with category fluency performance. We then employed a tractography-based approach in order to reveal regions that were structurally disconnected by the lesion and

assess their relationship with category fluency performance as compared to controls and other patients. Functional connectivity from the disconnected regions revealed large networks of interconnected areas. Within these regions/networks, measures of cortical thickness and of entropy of the rs-*f*MRI images were correlated to fluency performance, suggesting that some microstructural changes that occurred within these networks were due to the remote effect of a lesion that led to cognitive impairments. Consequently, the BCBtoolkit provided investigators with an ability to quantify the effect of brain damage upon the whole-brain, and explore its relationship to behavioural and cognitive abilities.

The investigation into the contribution of white matter tract disconnection is more than a century old approach and hypothesizes an interruption in the course of white matter tracts in single case patients (Lichtheim, 1885; Catani and ffytche, 2005). Our method provides an anatomical rationale, as well as puts forth a statistical methodology enabling it to be extended to group studies. In the case of category fluency performance, this analysis revealed a significant involvement of the anterior and long segments of the arcuate fasciculus, which are implicated in the language network (Catani and ffytche, 2005; Dronkers *et al.*, 2007; Forkel *et al.*, 2014). However, these tracts have been defined by their shape for convenience (e.g. uncinate for hook-shaped connections or arcuate for arched-shaped connections) and should not be considered as a single unit, as ultimately, sub-portions could contribute differently to the elaboration of the cognition and behaviour.

Data driven maps of disconnection or 'disconnectomes' were consequently produced in order to identify the sub-portion of disconnected tracts and reveal the pattern of cortico-subcortical areas that were disconnected by the lesion. For the first time, we exemplify that this method can go beyond assessing only lesions, and be employed to assess the relationship between disconnected areas and the patient's neuropsychological performance. Here, this approach revealed that category fluency performance was significantly decreased, when several cortical and subcortical clusters were directly disconnected. The observed areas are consistent with previous lesion studies on fluency tasks (MacPherson *et al.*, 2015). Furthermore, each area identified as significantly involved in this analysis corresponded, almost systematically, to activation loci derived from *f*MRI studies in healthy controls performing fluency and/or categorisation tasks. This result suggests that the method appropriately identified altered

functional networks contributing to the category fluency test. Nonetheless, one might argue that a cascade of polysynaptic events can influence behaviour and that dysfunctional, disconnected areas will also impact other indirectly connected areas.

In order to explore this additional dimension, we calculated the functional connectivity of the previously identified disconnected regions. In the case of the present analysis on category fluency performance, we revealed that the disconnected areas belonged to 3 large functional networks: a left dominant ventral fronto-parietal network, a mirror of the right-lateralized ventral attention network (Fox *et al.*, 2006), which link key language territories (Smith *et al.*, 2009) and is associated with executive functions (Power and Petersen, 2013; Parlatini *et al.*, 2017). We additionally showed the involvement of the cingulo-opercular network, a network that interacts with the fronto-parietal control network for the control of goal-directed behaviors (Gratton *et al.*, 2016), which together with cortico-striatal network may also be linked to a reduced performance in fluency tasks (Chouiter *et al.*, 2016). The cingulo-opercular and cortico-striatal networks may also have contributed to performance through the global inertia or the ability of participants to allocate and coordinate resources during the task (Bonnelle *et al.*, 2012). Finally, disconnection was associated with a significant reduction of functional connectivity in 2 out of the 3 networks investigated. This is an important result, as functional connectivity appeared to be less significantly impaired in bilateral networks, suggesting that the proportion of the preserved functional network in both of the intact hemispheres may contribute to the strength of functional connectivity.

Changes in connectivity should induce changes in the microstructure of the areas of projection, and provoke cognitive or behavioral consequences. Measures of the cortical thickness revealed a significant thinning for some, but not all, directly disconnected areas. This result may reflect a potential apoptosis mechanism. However, current limitations in spatial resolution and magnetic resonance imaging signal might have biased this measure in some regions due to changes in myelination in the lower layers of the cortex (Wagstyl *et al.*, 2015). Cortical thickness analyses revealed that the left dominant ventral fronto-parietal network, whether it is seeded from MFg, IPs or subcortical structures in the left hemisphere, had a reduced cortical thickness which was proportional to the category fluency performance. This result indicates a strong and encouraging relationship between the integrity of a network

derived from measures of cortical thickness and behavioural performances. Future research can benefit from this approach to stratify patients' population and predict potential recovery. Additionally, we explored whether synaptic and dendritic degeneration could also be captured by measures of rs-*f*MRI entropy, as a gage to quantify the complexity of local blood oxygen level density (BOLD) across time. Although this was highly significant when patients were compared to controls, the result between patients (connected and disconnected patients) did not survive the correction for multiple comparisons, indicating that BOLD may be too noisy of a measure to capture such fine microstructural events with high statistical power.

Overall, using the BCBtoolkit, researchers and clinicians can measure distant effects of brain lesions and associate these effects with neuropsychological outcomes. Taken together, these neuroimaging measures help discern the natural history of events occurring in the brain after a lesion, as well as assist in the localization of functions. These methods, gathered in the BCBtoolkit, are freely available as **supplementary software** at http://toolkit.bcblab.com

Authors contribution

C.F. implemented the methods inside the BCBtoolkit, performed the analyses and wrote the manuscript. L.C. created the pipeline for the preprocessing of the resting state and for the functional correlation and revised the manuscript. S.K. conceived and help to upgrade the statistical analyses. C.R. collected the neuroimaging data. M.U. and E.V recruited the subjects, collected and built the database of patients and matched healthy controls including the neuropsychological and neuroimaging data and revised the manuscript. E.V. also participated in the conception of the lesion study, and also provided funding for the database acquisition. R.L. provided funding for the study and revised the manuscript. M.T.d.S. wrote the manuscript, provided funding, conceived and coordinated the study, reviewed and collected neuroimaging data.

Acknowledgments

We thank Lauren Sakuma, Roberto Toro, Jean Dauniseau, Emmanuel Mandonnet, Beatrice Garcin, Stephanie J. Forkel and the BCBlab for useful discussions. The authors also thank the participants of this study as well as Prof. Claude Adam, Dr. Carole Azuar, Dr Marie-Laure

Bréchemier, Dr. Dorian Chauvet, Dr Frédéric Clarençon Dr. Vincent Degos, Prof. Sophie Dupont, Prof. Damien Galanaud, Dr Béatrice Garcin, Dr. Florence Laigle, Dr Marc-Antoine Labeyrie, Dr. Anne Leger, Prof. Vincent Navarro, Prof. Pascale Pradat-Diehl, and Prof. Michel Wager for their help in recruiting the patients. The research leading to these results received funding from the "Agence Nationale de la Recherche" [grants number ANR-09-RPDOC-004-01 and number ANR-13- JSV4-0001-01] and from the Fondation pour la Recherche Médicale (FRM). Additional financial support comes from the program "Investissements d'avenir" ANR-10-IAIHU-06.

References

Avants BB, Tustison NJ, Song G, Cook PA, Klein A, Gee JC. A reproducible evaluation of ANTs similarity metric performance in brain image registration. Neuroimage 2011; 54(3): 2033-44.

Badre D, Hoffman J, Cooney JW, D'Esposito M. Hierarchical cognitive control deficits following damage to the human frontal lobe. Nat Neurosci 2009; 12(4): 515-22.

Bates E, Wilson S, Saygin A, Dick F, Sereno MI, Knight RT, *et al*. Voxel-based lesion-symptom mapping. Nature Neuroscience 2003; 6(5): 448-50.

Bird CM, Malhotra P, Parton A, Coulthard E, Rushworth MF, Husain M. Visual neglect after right posterior cerebral artery infarction. J Neurol Neurosurg Psychiatry 2006; 77(9): 1008-12.

Bonnelle V, Ham TE, Leech R, Kinnunen KM, Mehta MA, Greenwood RJ, *et al*. Salience network integrity predicts default mode network function after traumatic brain injury. Proc Natl Acad Sci U S A 2012; 109(12): 4690-5.

Bredesen DE. Neural apoptosis. Ann Neurol 1995; 38(6): 839-51.

Broca P. Perte de la parole, ramollissement chronique et destruction partielle du lobe antérieur gauche du cerveau. Bull Soc Anthropol 1861; 2: 235-8, 301-21.

Capurso SA, Calhoun ME, Sukhov RR, Mouton PR, Price DL, Koliatsos VE. Deafferentation causes apoptosis in cortical sensory neurons in the adult rat. J Neurosci 1997; 17(19): 7372-84.

Carrera E, Tononi G. Diaschisis: past, present, future. Brain 2014; 137(Pt 9): 2408-22.

Catani M, ffytche DH. The rises and falls of disconnection syndromes. Brain 2005; 128(Pt 10): 2224-39.

Chouiter L, Holmberg J, Manuel AL, Colombo F, Clarke S, Annoni JM, *et al*. Partly segregated cortico-subcortical pathways support phonologic and semantic verbal fluency: A lesion study. Neuroscience 2016; 329: 275-83.

Corbetta M, Kincade MJ, Lewis C, Snyder AZ, Sapir A. Neural basis and recovery of spatial attention deficits in spatial neglect. Nature Neuroscience 2005; 8(11): 1603-10.

Coulthard EJ, Nachev P, Husain M. Control over conflict during movement preparation: role of posterior parietal cortex. Neuron 2008; 58(1): 144-57.

Damasio H, Damasio A. Lesion analysis in Neuropsychology. New York; 1989.

Das SR, Avants BB, Grossman M, Gee JC. Registration based cortical thickness measurement. Neuroimage 2009; 45(3): 867-79.

Dronkers NF, Plaisant O, Iba-Zizen MT, Cabanis EA. Paul Broca's historic cases: high resolution MR imaging of the brains of Leborgne and Lelong. Brain 2007; 130(Pt 5): 1432-41.

Dronkers NF, Wilkins DP, Van Valin RD, Jr., Redfern BB, Jaeger JJ. Lesion analysis of the brain areas involved in language comprehension. Cognition 2004; 92(1-2): 145-77.

Finger S, Koehler PJ, Jagella C. The Monakow concept of diaschisis: origins and perspectives. Arch Neurol 2004; 61(2): 283-8.

Forkel SJ, Thiebaut de Schotten M, Dell'Acqua F, Kalra L, Murphy DG, Williams SC, *et al.* Anatomical predictors of aphasia recovery: a tractography study of bilateral perisylvian language networks. Brain 2014; 137(Pt 7): 2027-39.

Fox MD, Corbetta M, Snyder A, Vincent JL, Raichle ME. Spontaneous neuronal activity distinguishes human dorsal and ventral attention systems. Proc Natl Acad Sci USA 2006; 103(26): 10046-51.

Geschwind N. Disconnexion syndromes in animals and man - Part I. Brain 1965a; 88: 237-94.

Geschwind N. Disconnexion syndromes in animals and man - Part II. Brain 1965b; 88: 585-644.

Gratton C, Neta M, Sun H, Ploran EJ, Schlaggar BL, Wheeler ME, *et al.* Distinct Stages of Moment-to-Moment Processing in the Cinguloopercular and Frontoparietal Networks. Cereb Cortex 2016.

Husain M, Kennard C. Visual neglect associated with frontal lobe infarction. J Neurol 1996; 243(9): 652-7.

Jenkinson M, Bannister P, Brady M, Smith S. Improved optimization for the robust and accurate linear registration and motion correction of brain images. Neuroimage 2002; 17(2): 825-41.

Jones DK, Griffin LD, Alexander DC, Catani M, Horsfield MA, Howard RJ, *et al.* Spatial normalization and averaging of diffusion tensor MRI data sets. NeuroImage 2002; 17(2): 592-617.

Jones DK, Simmons A, Williams SC, Horsfield MA. Non-invasive assessment of axonal fiber connectivity in the human brain via diffusion tensor MRI. Magnetic Resonance in Medecine 1999; 42(1): 37-41.

Karnath HO, Ferber S, Himmelbach M. Spatial awareness is a function of the temporal not the posterior parietal lobe. Nature 2001; 411(6840): 950-3.

Kinkingnehun S, Volle E, Pélégrini-Issac M, Golmard JL, Lehericy S, du Boisguéheneuc F, *et al.* A novel approach to clinical-radiological correlations: Anatomo-Clinical Overlapping Maps (AnaCOM): method and validation. NeuroImage 2007; 37(4): 1237-49.

Lezak M. Neuropsychological assessment. Oxford: Oxford University Press; 1995.

Lichtheim L. On aphasia. Brain 1885; 7: 433-84.

Logothetis N. What we can do and what we cannot do with fMRI. Nature 2008; 453(7197): 869-78.

MacPherson SE, Della Sala S, Cox S, Iveson MH. Handbook of Frontal Lobe Assessment. Oxford: Oxford University Press; 2015.

Mah YH, Husain M, Rees G, Nachev P. Human brain lesion-deficit inference remapped. Brain 2014; 137(Pt 9): 2522-31.

Mort DJ, Malhotra P, Mannan SK, Rorden C, Pambakian A, Kennard C, *et al.* The anatomy of visual neglect. Brain 2003; 126(Pt 9): 1986-97.

Nachev P, Coulthard E, Jager HR, Kennard C, Husain M. Enantiomorphic normalization of focally lesioned brains. Neuroimage 2008; 39(3): 1215-26.

Parlatini V, Radua J, Dell'Acqua F, Leslie A, Simmons A, Murphy DG, *et al.* Functional segregation and integration within fronto-parietal networks. Neuroimage 2017; 146: 367-75.

Power JD, Petersen SE. Control-related systems in the human brain. Curr Opin Neurobiol 2013; 23(2): 223-8.

Rojkova K, Volle E, Urbanski M, Humbert F, Dell'Acqua F, Thiebaut de Schotten M. Atlasing the frontal lobe connections and their variability due to age and education: a spherical deconvolution tractography study. Brain Struct Funct 2016; 221(3): 1751-66.

Rorden C, Karnath HO, Bonilha L. Improving lesion-symptom mapping. J Cogn Neurosci 2007; 19(7): 1081-8.

Sadaghiani S, D'Esposito M. Functional Characterization of the Cingulo-Opercular Network in the Maintenance of Tonic Alertness. Cereb Cortex 2015; 25(9): 2763-73.

Smith SM. Fast robust automated brain extraction. Hum Brain Mapp 2002; 17(3): 143-55.

Smith SM, Fox PT, Miller KL, Glahn DC, Fox PM, Mackay CE, *et al.* Correspondence of the brain's functional architecture during activation and rest. Proc Natl Acad Sci U S A 2009; 106(31): 13040-5.

Sokunbi MO, Fung W, Sawlani V, Choppin S, Linden DE, Thome J. Resting state fMRI entropy probes complexity of brain activity in adults with ADHD. Psychiatry Res 2013; 214(3): 341-8.

Thiebaut de Schotten M, Dell'Acqua F, Forkel SJ, Simmons A, Vergani F, Murphy DG, *et al.* A lateralized brain network for visuospatial attention. Nat Neurosci 2011; 14(10): 1245-6.

Thiebaut de Schotten M, Tomaiuolo F, Aiello M, Merola S, Silvetti M, Lecce F, *et al.* Damage to white matter pathways in subacute and chronic spatial neglect: a group study and 2 single-case studies with complete virtual "in vivo" tractography dissection. Cereb Cortex 2014; 24(3): 691-706.

Tustison NJ, Cook PA, Klein A, Song G, Das SR, Duda JT, *et al.* Large-scale evaluation of ANTs and FreeSurfer cortical thickness measurements. Neuroimage 2014; 99: 166-79.

Volle E, Kinkingnehun S, Pochon JB, Mondon K, Thiebaut de Schotten M, Seassau M, *et al.* The functional architecture of the left posterior and lateral prefrontal cortex in humans. Cereb Cortex 2008; 18(10): 2460-9.

Volle E, Levy R, Burgess PW. A new era for lesion-behavior mapping of prefrontal functions. In: D.T. S, Knight RT, editors. Principles of Frontal Lobe Function; 2013. p. 500–23.

Voorn P, Vanderschuren LJ, Groenewegen HJ, Robbins TW, Pennartz CM. Putting a spin on the dorsal-ventral divide of the striatum. Trends Neurosci 2004; 27(8): 468-74.

Wagstyl K, Ronan L, Goodyer IM, Fletcher PC. Cortical thickness gradients in structural hierarchies. Neuroimage 2015; 111: 241-50.

Woolrich MW, Jbabdi S, Patenaude B, Chappell M, Makni S, Behrens T, *et al.* Bayesian analysis of neuroimaging data in FSL. Neuroimage 2009; 45(1 Suppl): S173-86.

Yarkoni T, Poldrack RA, Nichols TE, Van Essen DC, Wager TD. Large-scale automated synthesis of human functional neuroimaging data. Nat Methods 2011; 8(8): 665-70.

Zhang Y, Brady M, Smith SM. Segmentation of brain MR images through a hidden Markov random field model and the expectation-maximization algorithm. IEEE Trans Med Imaging 2001; 20: 45–57.

Captions

Fig. 1: Category fluency performance (mean performance with 95% confidence intervals) for patients with (dark grey) or without (light grey) disconnection of each tract of interest. The green intervals indicate the range of controls performance corresponding to 95% confidence intervals. * $p < 0.05$ Bonferroni-Holms corrected for multiple comparisons.

Fig. 2: Areas directly disconnected by the lesion that significantly contributed to a decreased score on category fluency task (referred to as "disconnected areas" in the manuscript). a) Representative slices from disconnectome maps computed for category fluency performance, blue clusters indicate group average low performance and red high performance. b) Brain areas contributing significantly after correction for multiple comparison. c) Category fluency performance (mean performance with 95% confidence intervals) for patients with (dark grey) or without (light grey) disconnection of each of the examined cortical regions. The green interval indicates performance in matched controls with 95% confidence intervals. preSMA: presupplementary motor area, IPs: intraparietal sulcus, MFg: middle frontal gyrus, pars Op.: frontal pars opercularis, A: anterior group of thalamic nuclei, VA ventral anterior VLp: ventrolateral posterior, VLa: ventrolateral anterior. * $p < 0.05$ Bonferroni-Holms corrected for multiple comparisons.

Fig. 3: Areas classically activated with *f*MRI ($p< 0.01$ FDR corrected) during fluency (pink) and categorization (cyan) tasks. Areas involved in both fluency and categorization are highlighted in dark blue.

Fig. 4: Functional networks involving the identified disconnected areas, as defined by resting state functional connectivity. Top panel, main cortical networks involving the disconnected areas revealed by a principal component analysis. Bottom left panel, principal component analysis of the raw functional connectivity result. Bottom right panel, strength of the functional connectivity for patients with (dark grey) or without (light grey) involvement of the functional network. CO: Cingulo-opercular network, CS: cortico-striatal network, VFP:

Ventral fronto-parietal network. * indicates $p < 0.05$; **, $p < 0.01$

Fig. 5: Dimensional relationship between cortical thickness measured in rs-*f*MRI disconnected networks and category fluency. Regression lines are indicated in black and light red intervals correspond to mean confidence intervals. All significant networks appeared to belong to the VFP represented in the lower right panel.

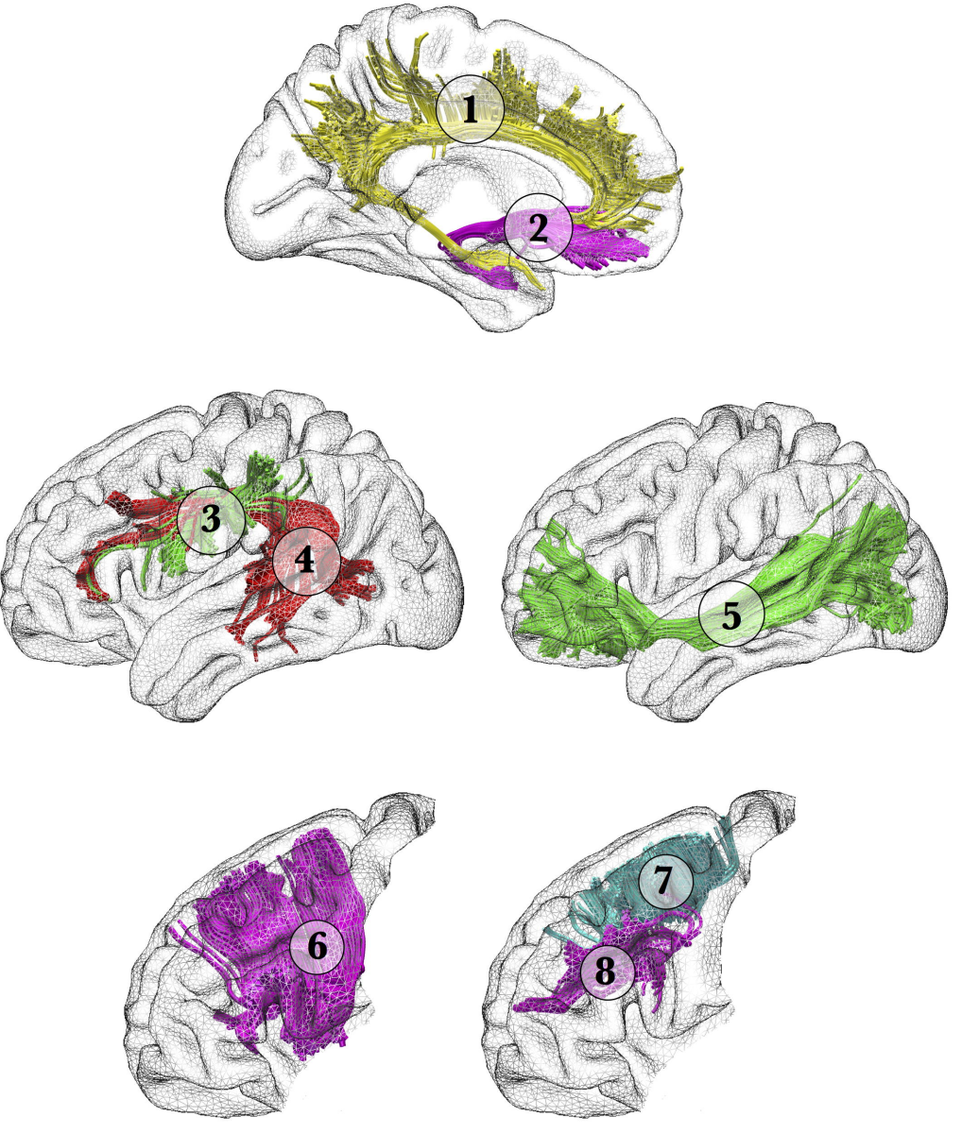
1
2
3
4
5
6
7
8

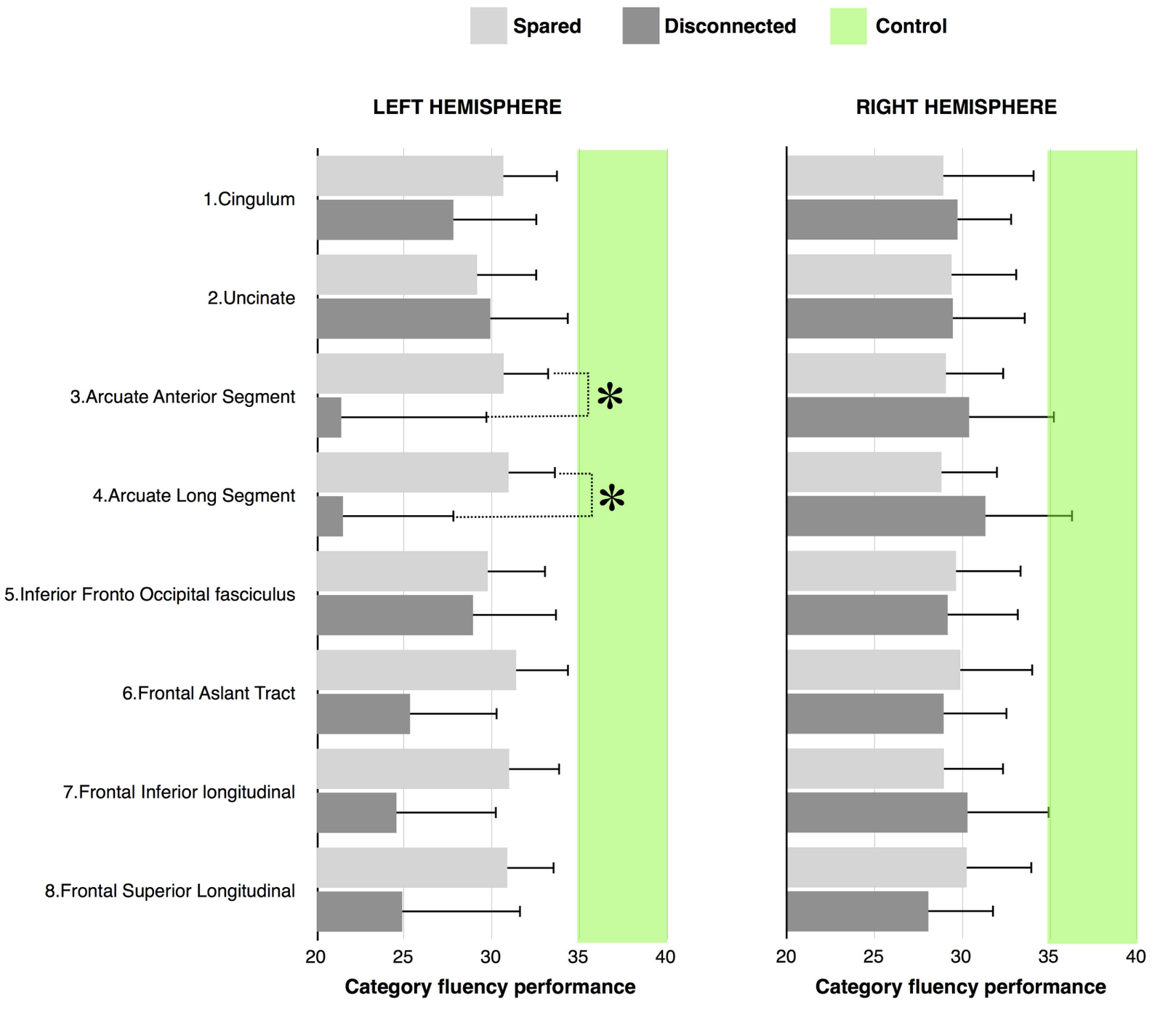
Spared
Disconnected
Control
LEFT HEMISPHERE
RIGHT HEMISPHERE
1.Cingulum
2.Uncinate
3.Arcuate Anterior Segment
4.Arcuate Long Segment
5.Inferior Fronto Occipital fasciculus
6.Frontal Aslant Tract
7.Frontal Inferior longitudinal
8.Frontal Superior Longitudinal
*
*
20
25
30
35
40
Category fluency performance
20
25
30
35
40
Category fluency performance

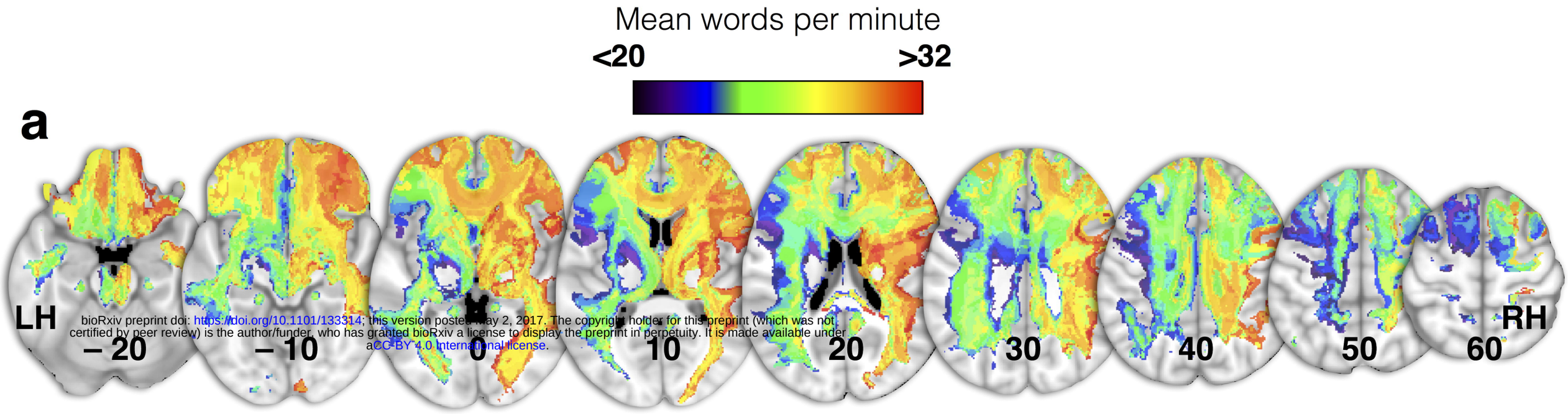

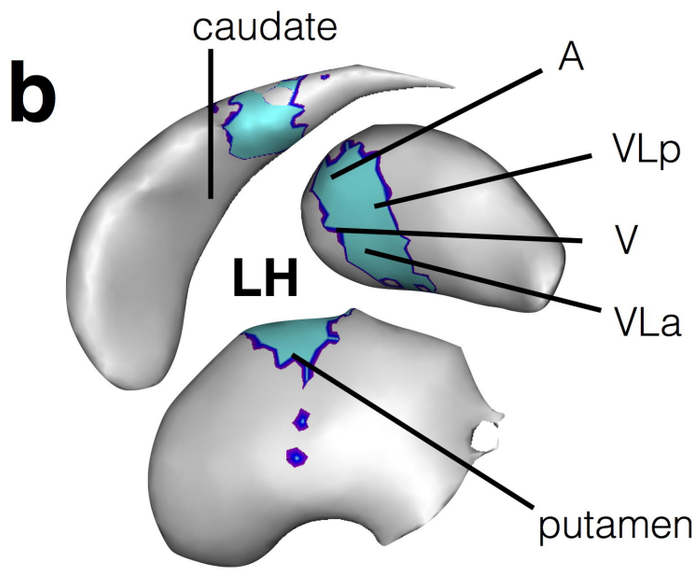

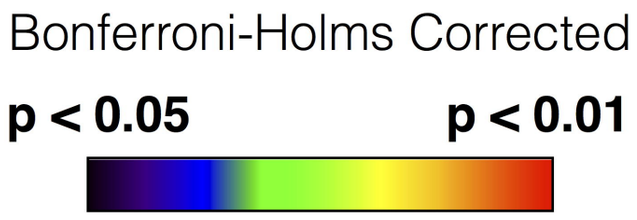

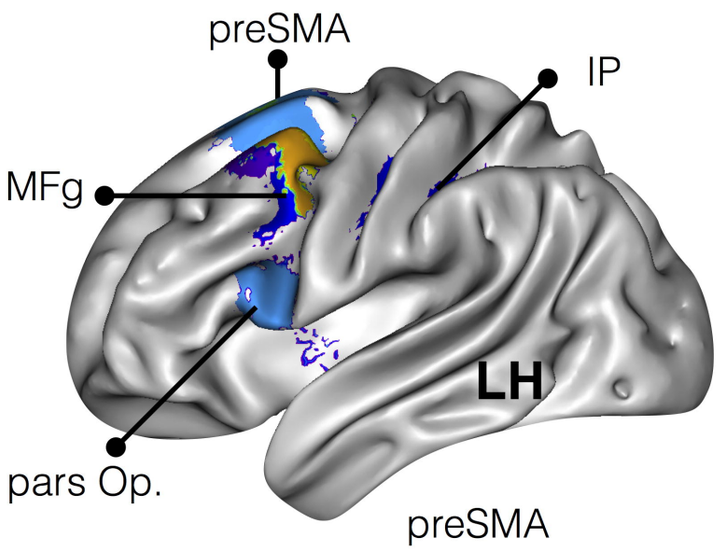

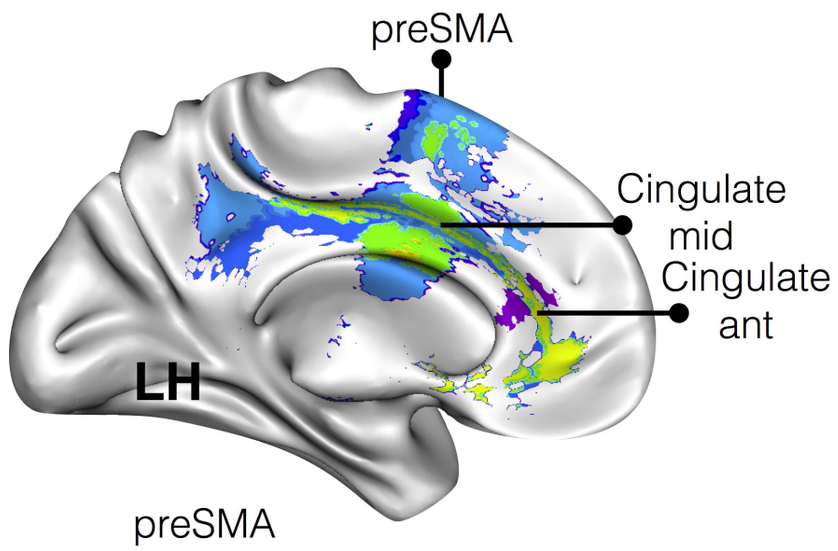

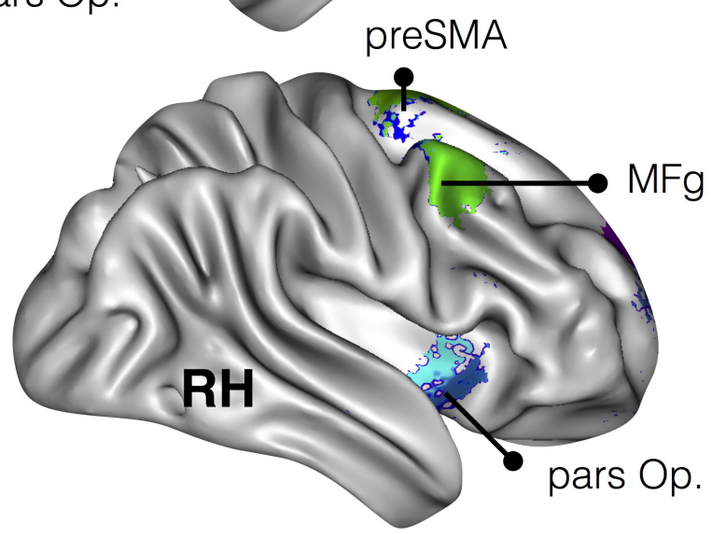

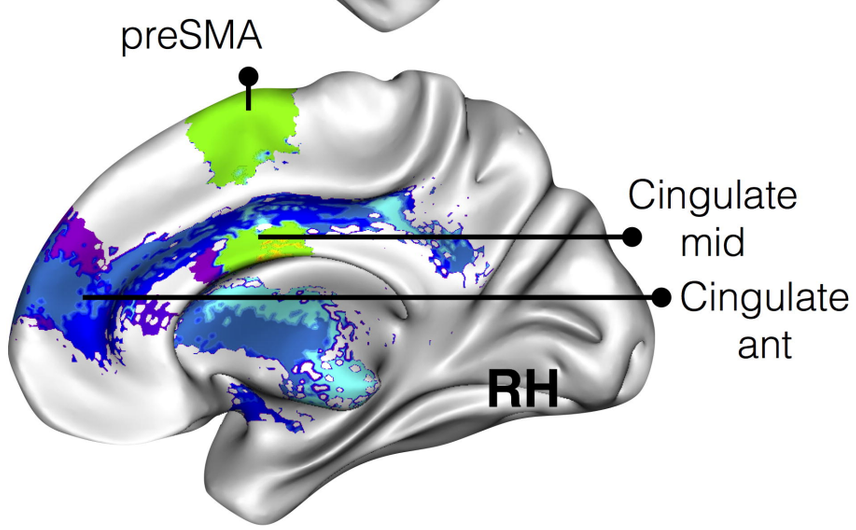

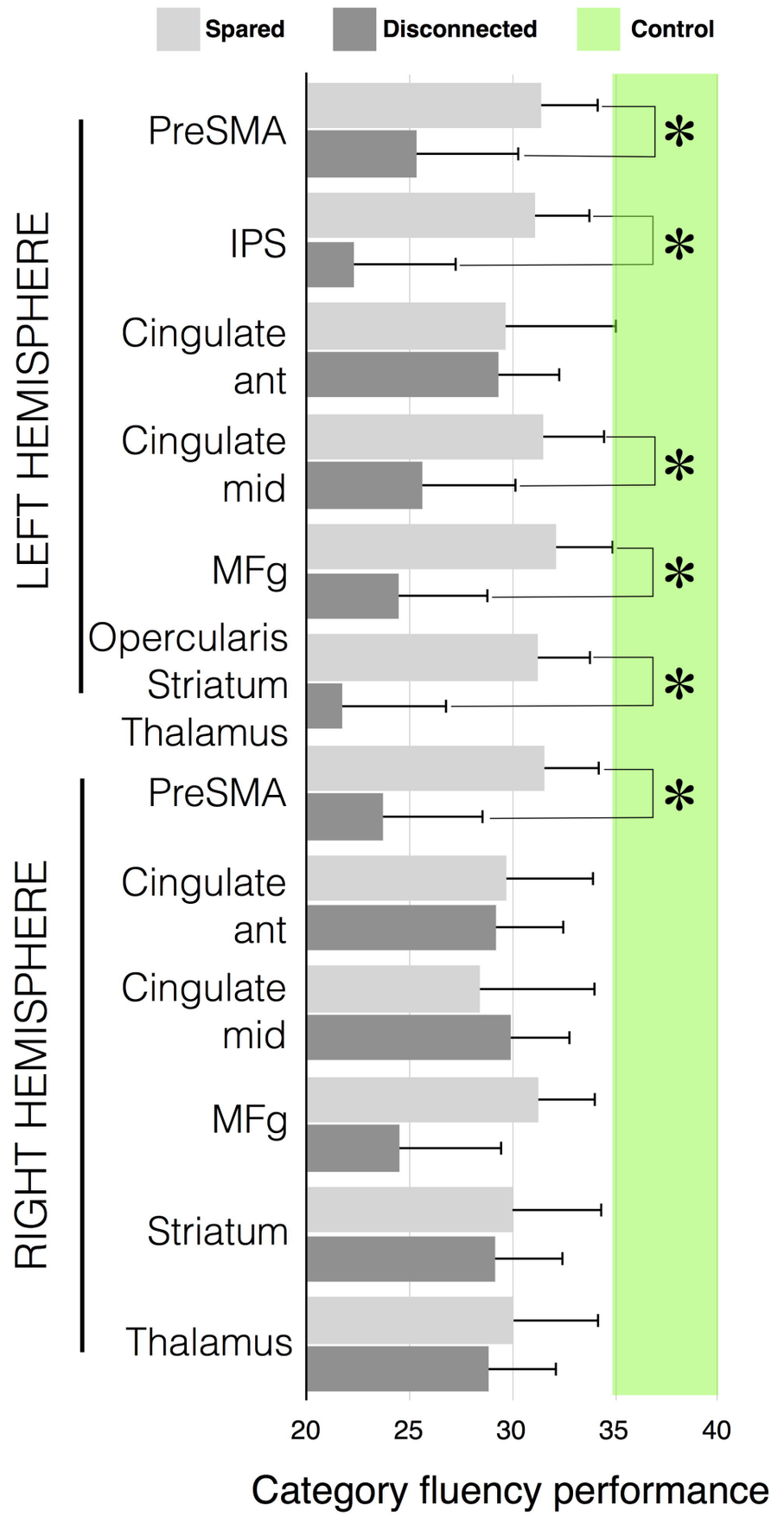

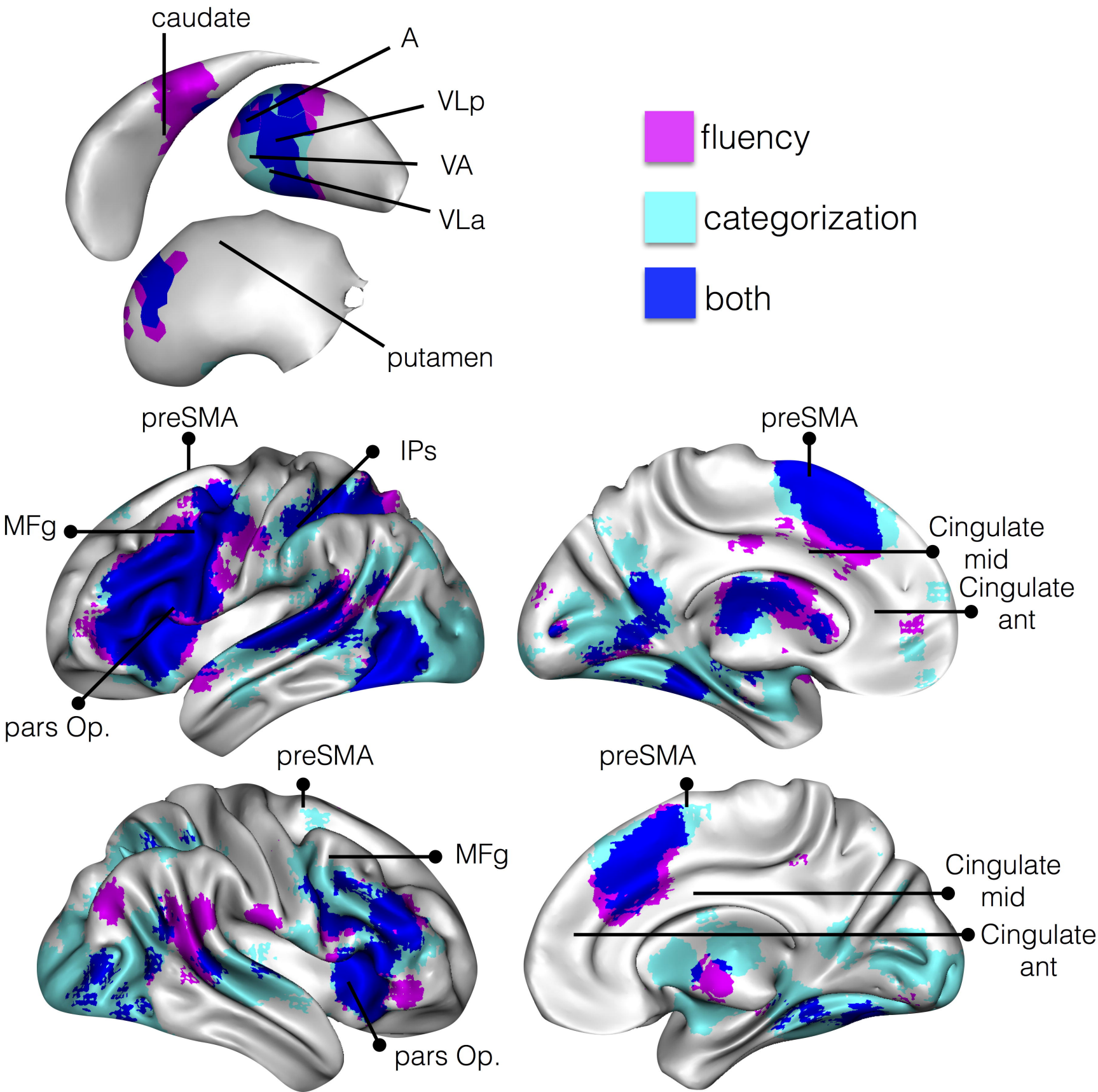
caudate
A
VLp
VA
VLa
putamen
fluency
categorization
both
preSMA
IPs
MFg
pars Op.
preSMA
Cingulate
mid
Cingulate
ant
preSMA
MFg
pars Op.
preSMA
Cingulate
mid
Cingulate
ant

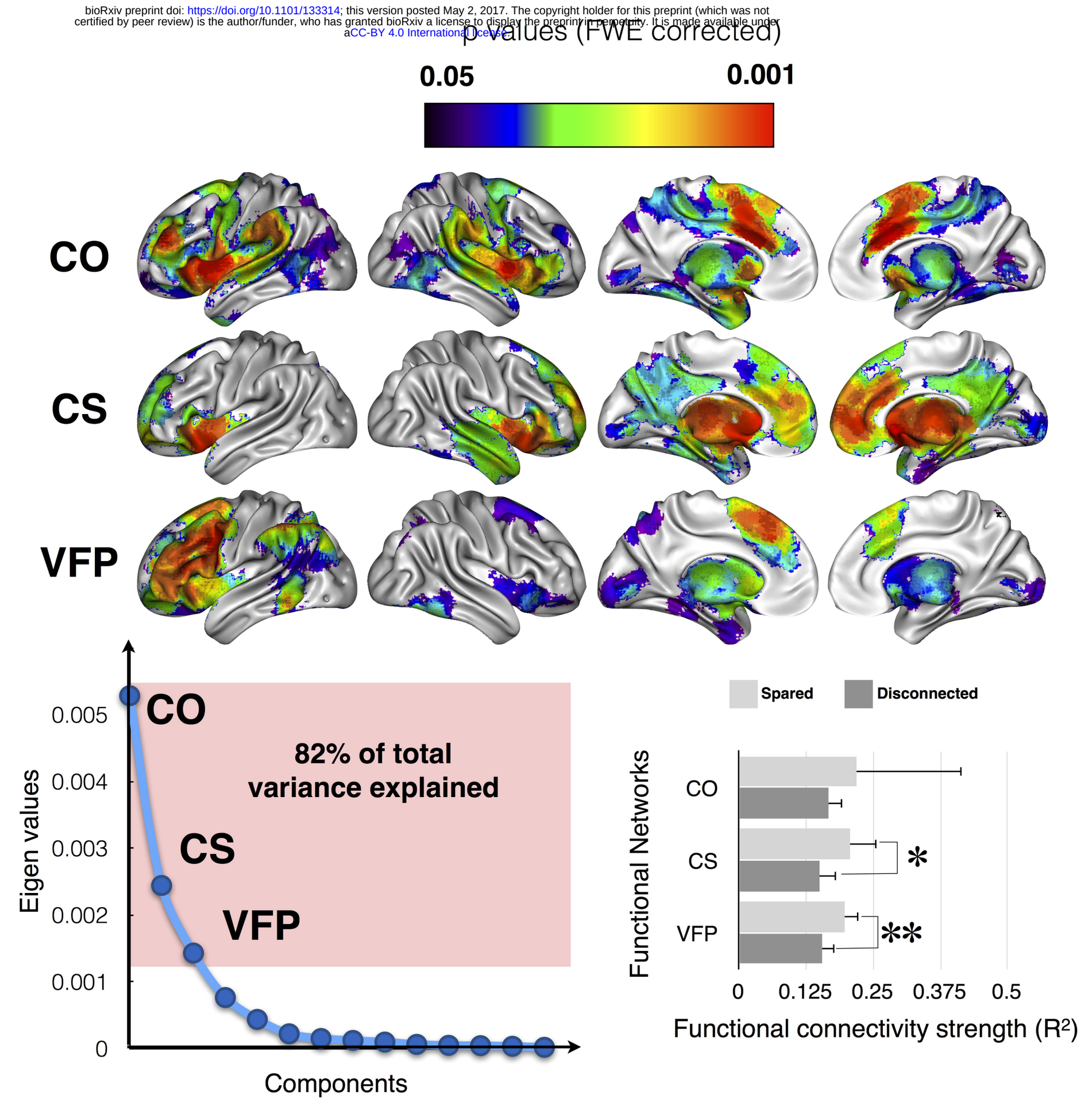

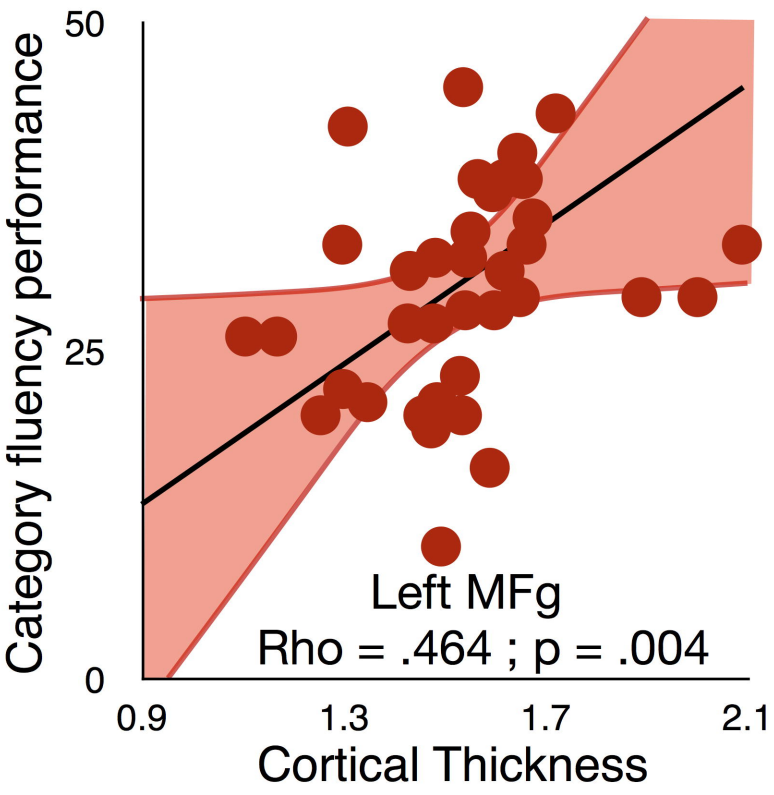
50
25
0
Category fluency performance
Left MFg
Rho = .464 ; p = .004
0.9
1.3
1.7
2.1
Cortical Thickness

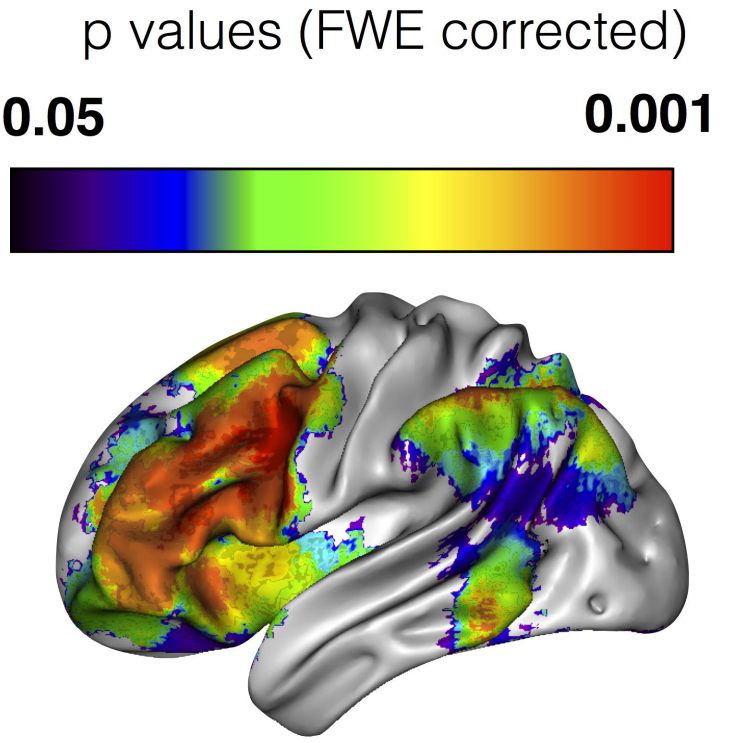
p values (FWE corrected)
0.05
0.001

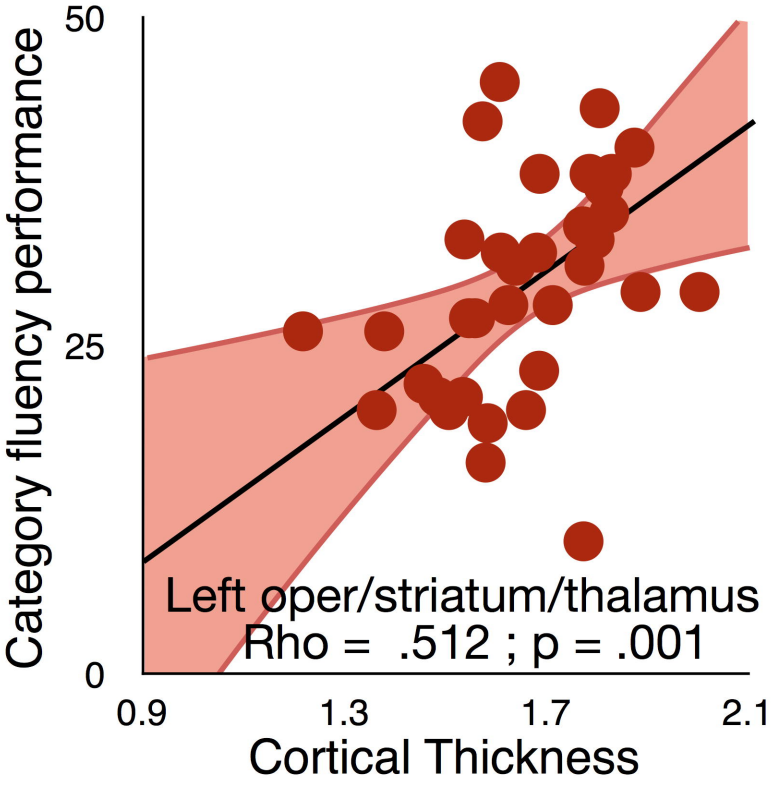
50
25
0
Category fluency performance
Left oper/striatum/thalamus
Rho = .512 ; p = .001
0.9
1.3
1.7
2.1
Cortical Thickness

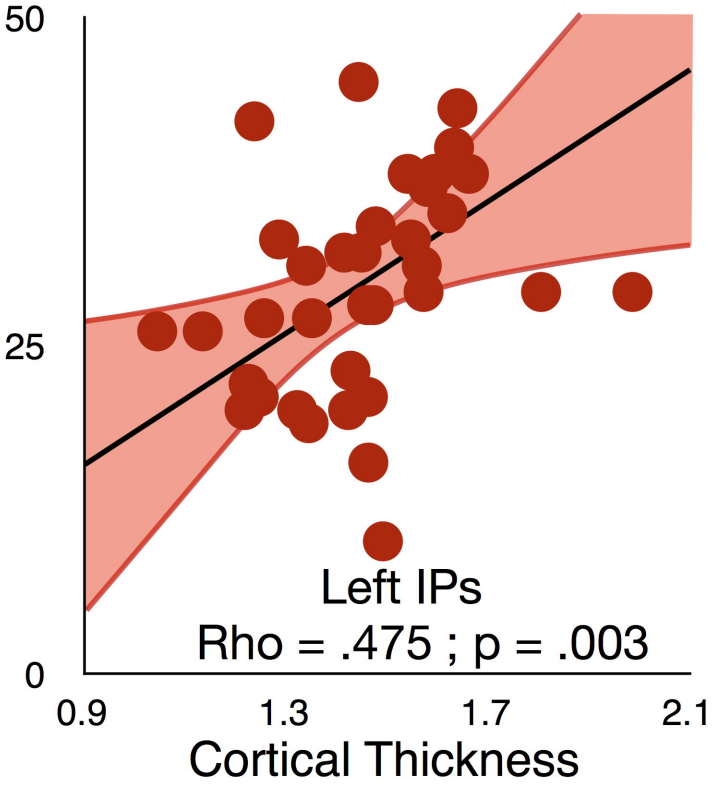
50
25
0
Left IPs
Rho = .475 ; p = .003
0.9
1.3
1.7
2.1
Cortical Thickness

Table 1: White matter tracts disconnection relationship with category fluency statistical report. Results are Bonferroni-Holms corrected for multiple comparisons.

	3 groups comparison		Patients disconnected and connected		Patients disconnected and controls		Patients connected and controls	
Tracts	Kruskal Wallis	P value	Mann Witney	P value	Mann Witney	P value	Mann Witney	P value
Cingulum Left	19	0.0001	141	0.2713	189	0.0006	277	0.0004
Cingulum Right	19	0.0001	161	NS	280	0.0003	187	0.0019
Uncinate Left	19	0.0001	148	0.4564	176	0.0027	291	0.0003
Uncinate Right	19	0.0003	167	NS	209	0.0006	258	0.0006
Arcuate Anterior Segment Left	22	0.0001	29	0.0465	12	0.0006	454	0.0003
Arcuate Anterior Segment Right	19	0.0004	126	NS	118	0.0029	348	0.0002
Arcuate Long Segment Left	23	0.0001	32	0.0465	13	0.0004	453	0.0004
Arcuate Long Segment Right	19	0.0005	107	NS	117	0.0068	349	0.0002
Inferior Fronto Occipital fasciculus Left	19	0.0001	165	0.5	196	0.0013	271	0.0003
Inferior Fronto Occipital fasciculus Right	19	0.0002	157	NS	199	0.0005	268	0.0007
Frontal Aslant Tract Left	21	0.0001	90	0.0622	90	0.0004	377	0.0004
Frontal Aslant tract Right	19	0.0006	155	NS	194	0.0003	272	0.0014
Frontal Inferior longitudinal Left	21	0.0001	69	0.0577	54	0.0004	413	0.0004
Frontal Inferior longitudinal Right	19	0.0004	140	NS	171	0.0029	295	0.0001
Frontal Superior Longitudinal Left	20	0.0001	75	0.0622	73	0.0006	393	0.0004
Frontal Superior Longitudinal Right	19	0.0005	129	NS	120	0.0003	346	0.0007

Table 2: Cortical thickness and *f*MRI entropy measures in disconnected areas. Uncorrected P values**.**

		3 groups comparison		Patients disconnected and connected		Patients disconnected and controls		Patients connected and controls	
	Disocnnected areas	Kruskal Wallis	P value	Mann Witney	P value	Mann Witney	P value	Mann Witney	P value
CORTICAL THICKNESS LEFT HEMISPHERE	PreSMA	8	0.0224	109	0.0944	168	0.0057	514	0.0565
	IPs	9	0.0131	54	0.0251	59	0.0019	667	0.1134
	Cingulate ant	5	0.0822	110	0.1000	465	0.0175	269	0.2061
	Cingulate mid	5	0.0759	139	0.2998	278	0.1436	435	0.0137
	MFg	8	0.0143	109	0.0695	172	0.0028	502	0.0710
	Opercularis	13	0.0012	40	0.0061	44	0.0006	583	0.0225
CORTICAL THICKNESS RIGHT HEMISPHERE	PreSMA	4	0.1328	134	0.4931	214	0.1711	523	0.0254
	Cingulate ant	7	0.0296	167	0.4696	362	0.0191	295	0.0169
	Cingulate mid	23	0.0000	61	0.0020	223	0.1414	254	0.1415
	MFg	6	0.0587	116	0.2634	163	0.0359	538	0.0359
SHANNON ENTROPY LEFT HEMISPHERE	PreSMA	24	0.0000	86	0.2171	85	0.0004	210	0.0000
	IPs	27	0.0000	40	0.0422	18	0.0002	260	0.0000
	Cingulate ant	44	0.0000	84	0.1158	109	0.0000	3	0.0000
	Cingulate mid	36	0.0000	97	0.3029	45	0.0000	127	0.0000
	MFg	16	0.0004	100	0.4246	125	0.0043	272	0.0003
	Opercularis, striatum, thalamus	17	0.0002	65	0.3680	75	0.0181	287	0.0001
SHANNON ENTROPY RIGHT HEMISPHERE	PreSMA	8	0.0177	82	0.2364	117	0.0078	413	0.0243
	Cingulate ant	55	0.0000	81	0.0640	16	0.0000	4	0.0000
	Cingulate mid	22	0.0000	111	0.4596	203	0.0001	114	0.0003
	MFg	22	0.0000	55	0.0497	136	0.0533	209	0.0000
	Striatum	23	0.0000	110	0.4436	202	0.0001	100	0.0001
	Thalamus	58	0.0000	67	0.0204	0	0.0000	6	0.0000